membranes

*Supplementary Materials*

# Optimizing Air Scouring Energy for Sustainable Membrane Bioreactor Operation by Characterizing the Combination of Factors Leading to Threshold Limiting Conditions

**Changyoon Jun [1,*], Kimia Aghasadeghi [2] and Glen T. Daigger [1]**

[1] Department of Civil and Environmental Engineering, University of Michigan, Ann Arbor, MI 48109, USA; gdaigger@umich.edu
[2] Fibracast Ltd., Hannon, ON L0R 1P0, Canada; kimia.aghasadeghi@fibracast.com
* Correspondence: cyjun@umich.edu

*Different Version of K Value Equations*

The initial idea regarding the relationship between velocity gradient and particle deposition tendency is described by Equation (S1). We have found that the total resistance term is essential to account for broader operational conditions and that the exponents for each side significantly affect the ability to distinguish limiting conditions from sub-limiting conditions, which is the key objective of this metric.

$$\kappa_1 \left( \frac{Q_A}{V \times \mu_{app}} \right)^{0.5} \geq \kappa_2 \frac{MLSS \times Q_P}{A} \quad \text{(S1)}$$

There were various experiments conducted to determine a better relationship by changing parameters and exponents on Equation (S1). These attempts are generally summarized by three distinct cases. First, rearranging Equation (S1) by $K_{Lim}$:

$$K_{1,Lim} \leq \frac{Q_A}{Q_P} \times \frac{a_s \times A}{MLSS^2 \times \mu_{app} \times Q_P} = K_1 \quad \text{(S2)}$$

The computed value of the right-hand side of Equation (S2) is referred to as $K_1$ ($\kappa_2^2/\kappa_1$), [$s^2$/(kg·m)].

Second, when the total resistance term ($R_T = (TMP \cdot A)/(\mu_w \cdot Q_P)$) is added to the right-hand side of Equation (S1) and rearranged by $K_{Lim}$, which gives:

$$K_{2,Lim} \leq \frac{Q_A}{Q_P} \times \frac{Q_P \times a_s \times \mu_w^2}{MLSS^2 \times \mu_{app} \times A \times TMP^2} = K_2 \quad \text{(S3)}$$

where $K_2$ (= $(\kappa_2/\kappa_1)^2$), [(m·$s^2$)/kg].

Lastly, when the $R_T$ term is added to the right-hand side, balances the exponents on both sides, and eliminates the squared root terms, resulting in Equation (S4):

$$\kappa_1 \times \frac{Q_A}{V \times \mu_{app}} \geq \kappa_2 \times MLSS \times \frac{Q_P}{A} \times R_T \quad \text{(S4)}$$

Equation S4 is then rearranged by $K_{Lim}$:

$$K_{3,Lim} \leq \frac{Q_A}{Q_P} \times \frac{a_s}{\mu_{app} \times MLSS} \times \frac{Q_P \times \mu_w}{TMP \times A} = K_3 \quad \text{(S5)}$$

where $K_{3,Lim} = \kappa_2/\kappa_1$, [(m·s)/kg], which is corresponding one to Equation (6) in main text.

*Comparison Results from Different K Value Equations*

Based on the differing behavior observed in Equations (S2), (S3), and (S5), the following two conditions were visually inspected:

$K_{Lim}$ represents a well-defined limiting condition and remains reasonably constant (i.e., its lower boundary is distinct from that of sub-limiting condition).

The general distribution of $K_{SubLim}$ is reasonably dispersed, with less skewness and a wider range of values, to allow for fine adjustments of the air flow according to the actual required air energy.

Figure S1 shows the variation of K values computed by Equation (S2) (i.e., $K_1$). Both trains of Plant A show a clear differentiation between $K_{Lim}$ and $K_{SubLim}$, with $K_{Lim}$ located at the lower boundary of K values. However, Plant B shows less distinct separation of limiting conditions, especially during periods when a larger number of limiting conditions is observed. This suggests that an operational condition with frequent fouling cannot be adequately explained if the total resistance term is not taken into consideration.

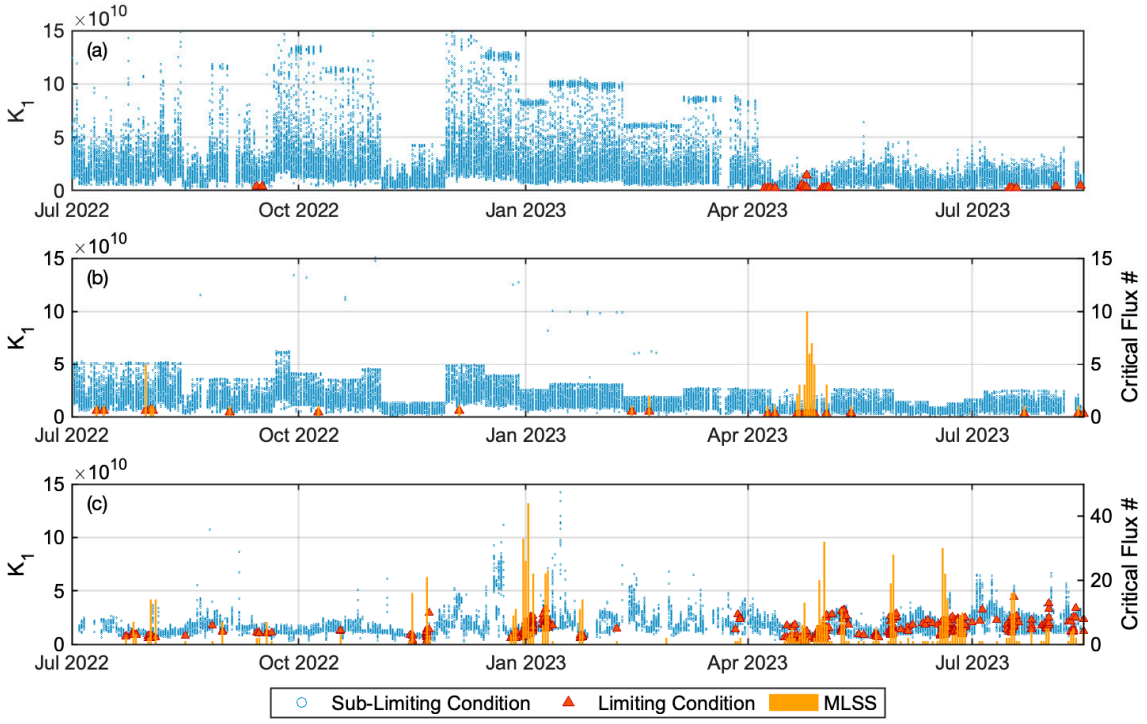


**Figure S1.** Time Series Variation of $K_1$ (Equation (S2)) in Limiting Condition (Red Square), Sub-Limiting Condition (Blue Circle), and Number of Observed Limiting Condition (Orange Bar) : (**a**) Plant A Train 1, (**b**) Plant A Train 2, and (**c**) Plant B Train 1.

In case of $K_2$ (Figure S2), $K_{Lim}$ is generally found at the lower bound of K values in both trains of Plant A and Plant B. Compared to $K_1$, $K_2$ has suppressed K values under higher TMP conditions, particularly in Plant B, and the increased vertical variation depends on MLSS (MLSS data is not shown here), suggesting a more sensitive variation to TMP and MLSS.

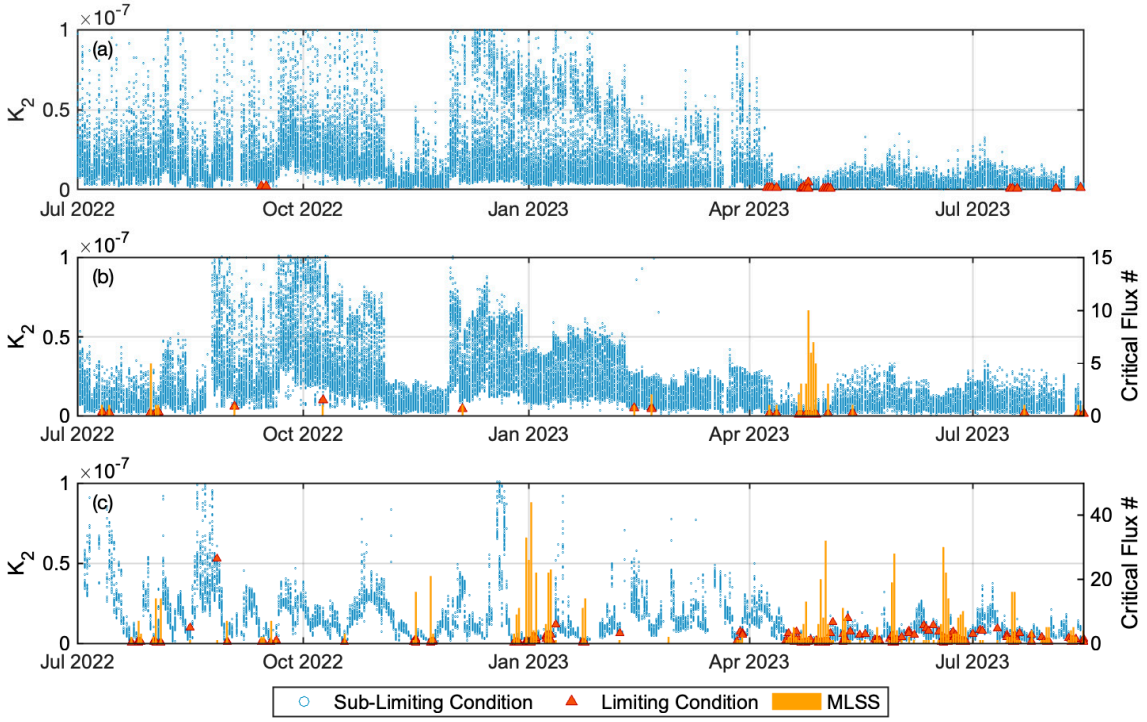


**Figure S2.** Time Series Variation of $K_2$ (Equation (S3)) in Limiting Condition (Red Square), Sub-Limiting Condition (Blue Circle), and Number of Observed Limiting Condition (Orange Bar) : (**a**) Plant A Train 1, (**b**) Plant A Train 2, and (**c**) Plant B Train 1.

$K_3$ has relatively lower sensitivity to MLSS and TMP, showing broader vertical variation of K values. This results in a clearer distinction between limiting conditions and sub-limiting conditions as shown in Figure S3.

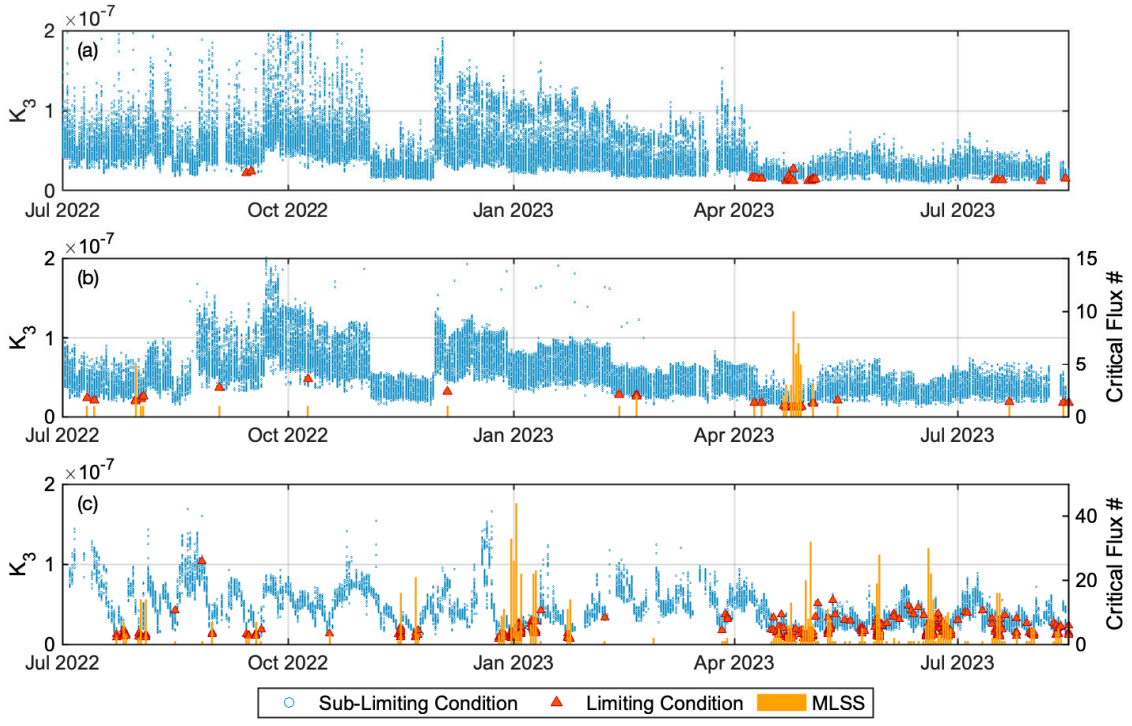

**Figure S3.** Time Series Variation of $K_3$ (Equation (S5)) in Limiting Condition (Red Square), Sub-Limiting Condition (Blue Circle), and Number of Observed Limiting Condition (Orange Bar): (**a**) Plant A Train 1, (**b**) Plant A Train 2, and (**c**) Plant B Train 1.

Upon closely inspecting $K_{Lim}$ and $K_{SubLim}$ using Kernel Density Estimation (KDE), it becomes apparent how well $K_{Lim}$ is distinguished between limiting and sub-limiting conditions. Visual inspection of the distributions indicates that $K_1$ has lower separation ability, especially in Plant B, where the means of the $K_{Lim}$ and $K_{SubLim}$ distributions are closely aligned.

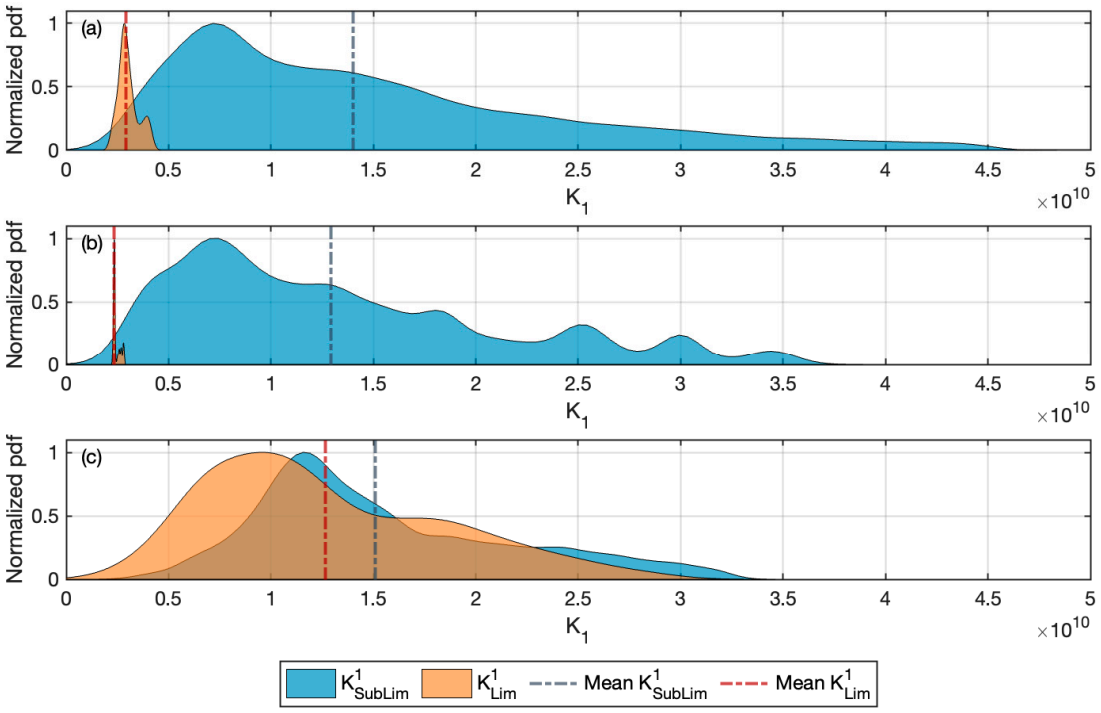


**Figure S4.** Comparison of Normalized Kernel Density Estimates for $K_1$ (Equation (S2)) for (**a**) Plant A Train 1, (**b**) Plant A Train 2, and (**c**) Plant B Train 1.

The KDE distribution for $K_{SubLim}$ is a skewed pattern toward to $K_{Lim}$, and both have a lower boundary near zero (Figure S5), which makes it less efficient to distinguish the $K_{Lim}$ distribution from the $K_{SubLim}$ distribution.

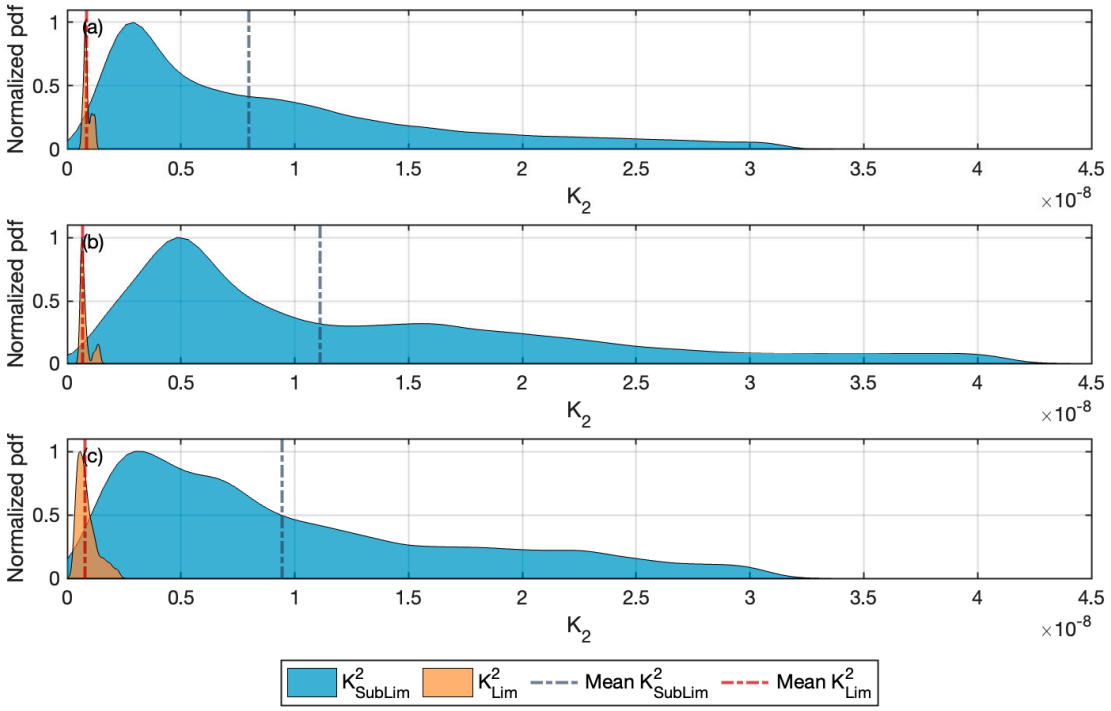


**Figure S5.** Comparison of Normalized Kernel Density Estimates for $K_2$ (Equation (S3)) for (**a**) Plant A Train 1, (**b**) Plant A Train 2, and (**c**) Plant B Train 1.

$K_3$ shows better distinction and clearer differences for both distributions, with less skewness and more reasonable horizontal variation of $K_{SubLim}$ based on mean of $K_{SubLim}$ as a central value.

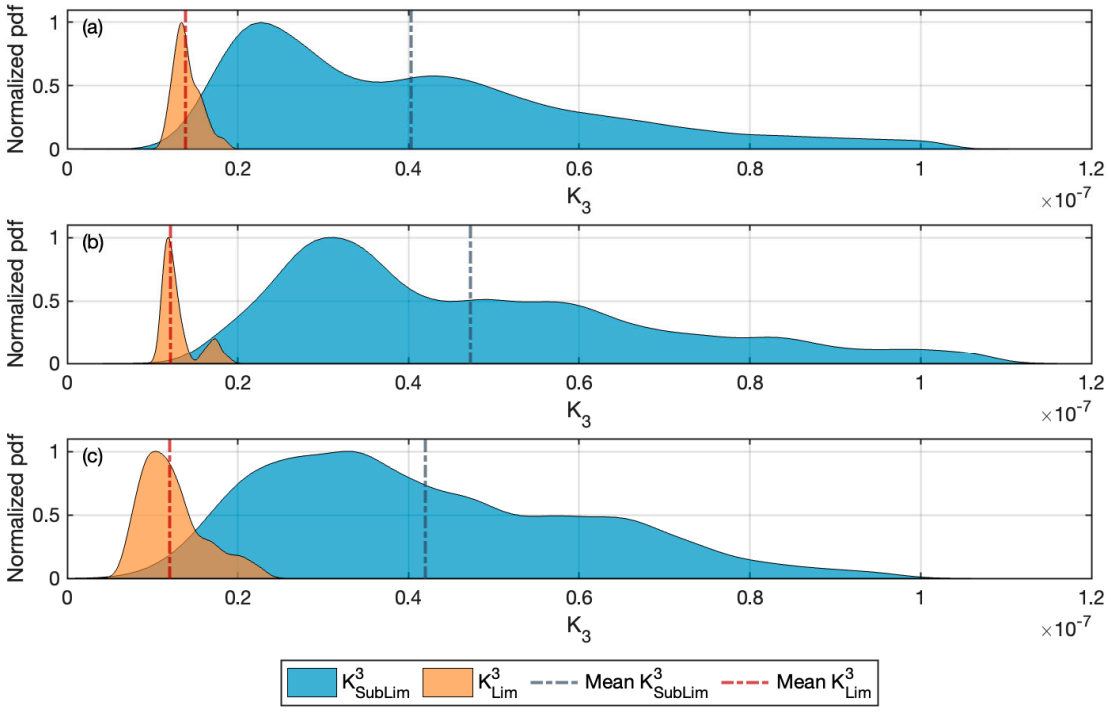


**Figure S6.** Comparison of Normalized Kernel Density Estimates for $K_3$ (Equation (S5)) for (**a**) Plant A Train 1, (**b**) Plant A Train 2, and (**c**) Plant B Train 1.

Visual inspection suggests that Equations S2, S3, and S5 produce different results distinguishing the limiting condition and estimating a reasonable variation of $K_{SubLim}$. Furthermore, it shows that $K_3$ performs better for these objectives than $K_1$ and $K_2$. To ensure a concise estimation of $K_{Lim}$, Coefficient of Variation (CV) is applied.

Table 1 summarizes the statistics for the determined $K_{Lim}$ values. A lower CV value indicates more concise estimations of $\widehat{K}_{Lim}$ and less variability. Among all other cases, $K_3$ shows better performance and thus supports the use of this equation for further investigation.

**Table S1.** Summary of Statistics of $K_{Lim}$ values in different scenarios.

| Plant ID | $K_{1,Lim}$ | | $K_{2,Lim}$ | | $K_{3,Lim}$ | |
|---|---|---|---|---|---|---|
| | **Mean (Std.)** | **CV** | **Mean (Std.)** | **CV** | **Mean (Std.)** | **CV** |
| Plant A T1 | $3.0 \times 10^{9}$ ($0.5 \times 10^{9}$) | 0.16 | $8.9 \times 10^{-10}$ ($1.7 \times 10^{-10}$) | 0.19 | $1.4 \times 10^{-8}$ ($0.2 \times 10^{-8}$) | 0.11 |
| Plant A T2 | $2.5 \times 10^{9}$ ($0.2 \times 10^{9}$) | 0.07 | $7.8 \times 10^{-10}$ ($2.5 \times 10^{-10}$) | 0.31 | $1.3 \times 10^{-8}$ ($0.2 \times 10^{-8}$) | 0.16 |
| Plant B T1 | $12.7 \times 10^{9}$ ($5.8 \times 10^{9}$) | 0.45 | $8.6 \times 10^{-10}$ ($4.4 \times 10^{-10}$) | 0.51 | $1.2 \times 10^{-8}$ ($0.3 \times 10^{-8}$) | 0.3 |

*Variation of Featured Variables in Limiting Conditions*

The featured variables (e.g., TMP, Flux, Permeability) corresponding to the extracted cycles in the detected limiting condition among three different datasets are illustrated in Figures S7 to S9. These figures effectively capture the moments of rapid resistance increase at the given flux, despite some ambiguity (i.e., possible false positive). Permeability [LMH/bar] is computed based on [47]. Note that for Plant B Train 1, due to the large number of cycles in the limiting condition, the extracted cycles are plotted at intervals of 20.

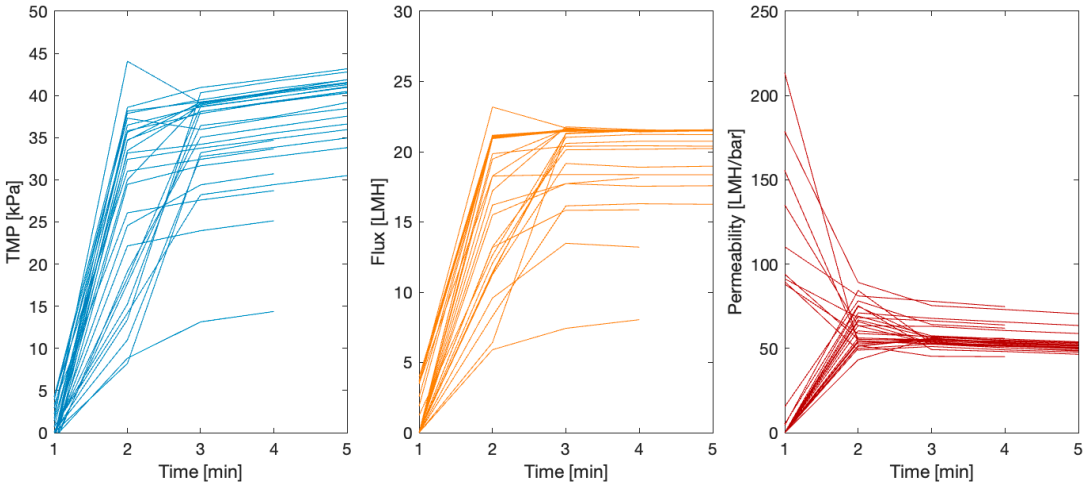


**Figure S7.** Extracted Cycles in Limiting Condition for Plant A Train 1.

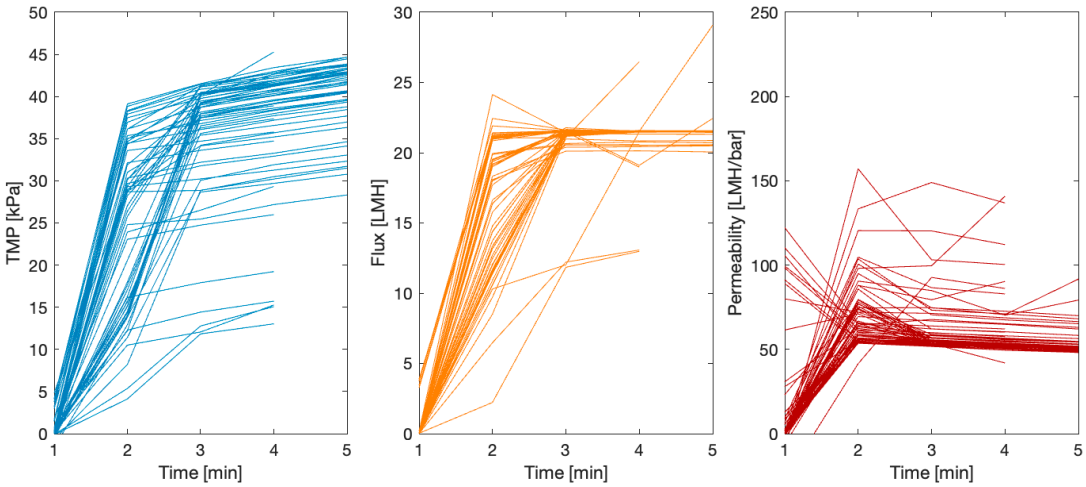


**Figure S8.** Extracted Cycles in Limiting Condition for Plant A Train 2.

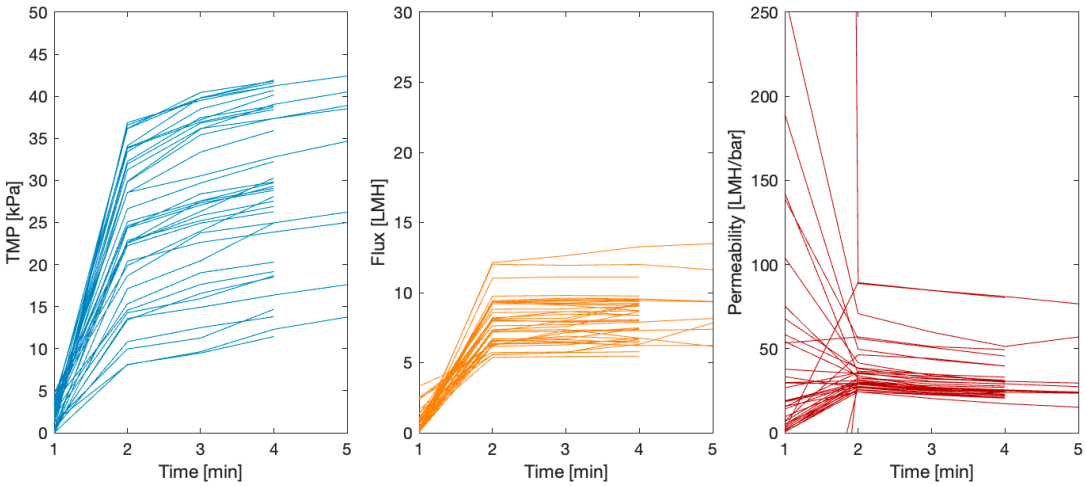


**Figure S9.** Extracted Cycles in Limiting Condition for Plant B Train 1.

## Reference

47. Key MBR operation and maintenance parameters – membrane side. Available online: https://www.thembrsite.com/membrane-processes-basics/membrane-bioreactor-operation-maintenance-flux-tmp-permeability-shear/#:~:text=The%20ratio%20of%20the%20flux,Imperial%20units%20of%20GFD%2Fpsi. (accessed on 31 January 2024).